PHILOSOPHICAL TRANSACTIONS OF THE ROYAL SOCIETY B BIOLOGICAL SCIENCES

Mapping the Dynamics of a Bursting Neuron

John Guckenheimer, Shay Gueron and Ronald M. Harris-Warrick

Phil. Trans. R. Soc. Lond. B 1993 **341**, 345-359
doi: 10.1098/rstb.1993.0121

Mapping the dynamics of a bursting neuron

JOHN GUCKENHEIMER[1,2], SHAY GUERON[2] AND RONALD M. HARRIS-WARRICK[3]

[1]*Mathematics Department and* [2]*Center for Applied Mathematics, 504 ETC Building, Cornell University, Ithaca, New York 14853, U.S.A.*

[3]*Section of Neurobiology and Behavior, S. G. Mudd Hall, Cornell University, Ithaca, New York 14853, U.S.A.*

SUMMARY

The anterior burster (AB) neuron of the lobster stomatogastric ganglion displays varied rhythmic behavior when treated with neuromodulators and channel-blocking toxins. We introduce a channel-based model for this neuron and show how bifurcation analysis can be used to investigate the response of this model to changes of its parameters. Two dimensional maps of the parameter space of the model were constructed using computational tools based on the theory of nonlinear dynamical systems. Changes in the intrinsic firing and oscillatory properties of the model AB neuron were correlated with the boundaries of Hopf and saddle-node bifurcations on these maps. Complex rhythmic patterns were observed, with a bounded region of the parameter plane producing bursting behavior of the model neuron. Experiments were performed by treating an isolated AB cell with 4-aminopyridine which selectively reduces g_A, the conductance of the transient potassium channel. The model accurately predicts the qualitative changes in the neuronal voltage oscillations that are observed over a range of reduction of g_A in the neuron. These results demonstrate the efficacy of dynamical systems theory as a means of determining the varied oscillatory behaviors inherent in a channel-based neural model. Further, the maps of bifurcations provide a useful tool for determining how these behaviors depend upon model parameters and comparing the model to a real neuron.

1. INTRODUCTION

The anterior burster (AB) neuron of the stomatogastric ganglion (STG) of the spiny lobster *Panulirus interruptus* is a conditional bursting neuron whose properties have been studied intensively (Harris-Warrick & Flamm 1987; Harris-Warrick & Johnson 1987). When isolated from other neurons, the AB cell is quiescent with a stable resting potential. Harris-Warrick and Johnson (1987) demonstrated that pharmacological blockade of several different potassium currents in this neuron can lead to rhythmic electrical activity. There are several characteristic patterns of rhythmic activity, including bursting oscillations, periodic action potentials of constant amplitude and slow oscillations without action potentials. This paper examines dynamical models for the AB cell. We introduce a new modeling strategy that is based upon multiparameter bifurcation theory, one of the developments of renewed interest in the behavior of nonlinear dynamical systems during the past two decades. Our primary purpose here is to demonstrate how these methods can produce detailed maps that partition a parameter space of a model into regions with different types of dynamical behavior. Comparisons of the behavior of the model neuron are made with a limited set of experimental data on a real neuron to illustrate how these maps allow us to select parameter values for which there is a good match between the rhythmic patterns in model and experimental data.

The models we use are based on a system of differential equations describing the activity of a set of ion channels present in the AB cell membrane. Our models are extensions of one introduced by Plant (1981), refined by Rinzel and Lee (1987), and used by Epstein and Marder (1990) as a representation of the electrical activity of the AB cell. Our work builds upon theirs in two ways: (i) we add a representation of the transient potassium A channel to their models; and (ii) we perform an extensive analysis of bifurcations in the model's parameter space, to show how the dynamics of the models depend upon variations of model parameters. The predictions of our model are compared more directly with experimental observations than the results of previous analyses.

Voltage clamp experiments were performed to measure the characteristics of the potassium and leak channels of the neuron (Golowasch 1991; Tierney *et al.* 1992). However, for technical reasons described below, attempts to voltage clamp inward currents in the AB cell *in situ* have not yet been successful. Instead, we used simulations and analysis of the model to find parameter values that reproduce the observed responses of the cell to different environments. We assume that a fundamental aspect of the real cell's function is its sensitivity to small stimuli. Therefore, we initially pick parameter values that lie in regions

Phil. Trans. R. Soc. Lond. B (1993) **341,** 345–359
Printed in Great Britain

where qualitative features of the model dynamics are sensitive to small changes in parameter values. This is accomplished by computing the location of degenerate bifurcations in the model. We are encouraged that the model does reproduce many of the changes in bursting behavior during pharmacological reduction in the conductances of potassium channels observed by Harris-Warrick and Johnson (1987) and in additional experiments that were conducted as a benchmark for comparison with these models.

Without this systematic strategy for locating relevant regions of the parameter space of our model corresponding to various behaviors, it would have been difficult to achieve such a successful comparison. Previous modeling studies have produced good fits to recorded experimental measurements under fixed experimental measurements, but they have seldom explored whether the effect of modulatory changes within an experiment can be faithfully reproduced within the model. Neural systems undergo large changes in their rhythmic properties with small changes in their inputs, and this correlates with radical alterations in behavior (Harris-Warrick & Marder 1991). Thus, the ability of models to produce similar appropriate changes with subtle changes in parameters is a fundamental aspect of their representation of neural behavior. Our work demonstrates the suitability of computational approaches to these questions based upon the bifurcation theory of dynamical systems.

2. CHANNELS AND NEURAL MODELS BASED ON CHANNELS

Changes in the electrical potential of a neuron are primarily due to ionic currents (I_j) that flow through channels located within the membrane. If the cell is isopotential, the membrane potential v satisfies the equation:

$$C_m\dot{v} = -\sum_j I_j + I_{ext}, \tag{1}$$

where C_m denotes the membrane capacitance, and experimentally imposed external currents are denoted by I_{ext}. The different currents are each represented by an equation of the general form

$$I_j = g_j a_j^p b_j^q (v - v_j), \tag{2}$$

where g_j is the maximal conductance, a_j is related to the probability that the channel is activated, b_j is related to the probability that the channel is inactivated and v_j is the reversal potential for the specific ion channel (Hille 1992).

The activation and inactivation processes respond to voltage changes by shifting towards a new steady state value. This steady state is voltage dependent and sometimes also depends on an ion concentration (e.g. calcium). We describe the time dependent equilibration by a typical differential equation of the form

$$\dot{a} = (a_\infty - a)K_a, \tag{3}$$

where K_a is the rate constant for the process and a_∞ is its (voltage dependent) steady state value. The activation steady state is represented by a sigmoid function

$$a_\infty(v) = \frac{1}{1 + e^{\frac{v - v_a}{s_a}}}. \tag{4}$$

Here v_a is the voltage where a_∞ attains the value $\frac{1}{2}$. The parameter s_a is the 'width' of the sigmoid curve (negative for activation and positive for inactivation processes). For two of the channels, we take the time constant K_a to be infinite, and replace the differential equation (3) by the equation $a = a_\infty$. The inactivation process is described by equations analogous to 3 and 4. In some cases the inactivation process (b) is described instead as a weighted average of two sigmoids (a_b,b_b) with a constant rate (λ_b)

$$\dot{b} = \lambda_b(a_b(1 - b) - b_b b). \tag{5}$$

Activation and inactivation often occur on different time scales. One can approximate processes that are faster than the time scales of interest as instantaneous and represent the corresponding variable only by its steady state value. This reduces the number of differential equations in the model.

We now enumerate the six specific currents that are incorporated into our model cell.

1. The basic properties of voltage-activated sodium channels were characterized in the work of Hodgkin and Huxley (Hodgkin & Huxley 1952). As in most subsequent models for electrical activity in nerve membranes, we use the Hodgkin-Huxley representation of sodium channels. The conductance is given by the expression $g_{Na}m^3h$, where g_{Na} represents the maximum conductance. The inactivation variable h is defined by the differential equation (9) (together with equations (15) and (16)) while the (faster) activation process m is assumed to be instantaneous and is defined by equations (12), (13) and (14). This common assumption simplifies the numerical analysis by reducing the stiffness of the resulting differential equations model and the dimension of its phase space. The sodium equilibrium potential is denoted v_{Na}. In figure 1*a* we have plotted the equilibrium values of m, h and m^3h as a function of v.

2. We have adopted the representation of calcium currents for the Aplysia R15 neuron used by Rinzel & Lee (1987). Equations (6), (7), (10) and (21) define I_{Ca}, with equilibrium potential v_{Ca} and maximal conductance g_{Ca}. The conductance of this channel is both calcium and voltage dependent. The activation variable, z, is a slow voltage dependent process shifting towards its steady state value (z_v) with constant rate τ_z (equation (10)). The inactivation process is assumed to respond instantaneously to calcium concentration and it is represented by $1/(0.5+c)$ (where c denotes the dimensionless activity of free calcium in the cell). Equation (7) describes the slow dynamics of the calcium concentration, governed by the rate constant ρ. In figure 1*b* we plot the voltage dependence of the steady state value of Ca from its kinetic equation (7) and the coefficient $z/(0.5+c)$ that modifies the conductance of the calcium current.

3. The voltage-dependent potassium current I_K

PHILOSOPHICAL TRANSACTIONS OF THE ROYAL SOCIETY B BIOLOGICAL SCIENCES

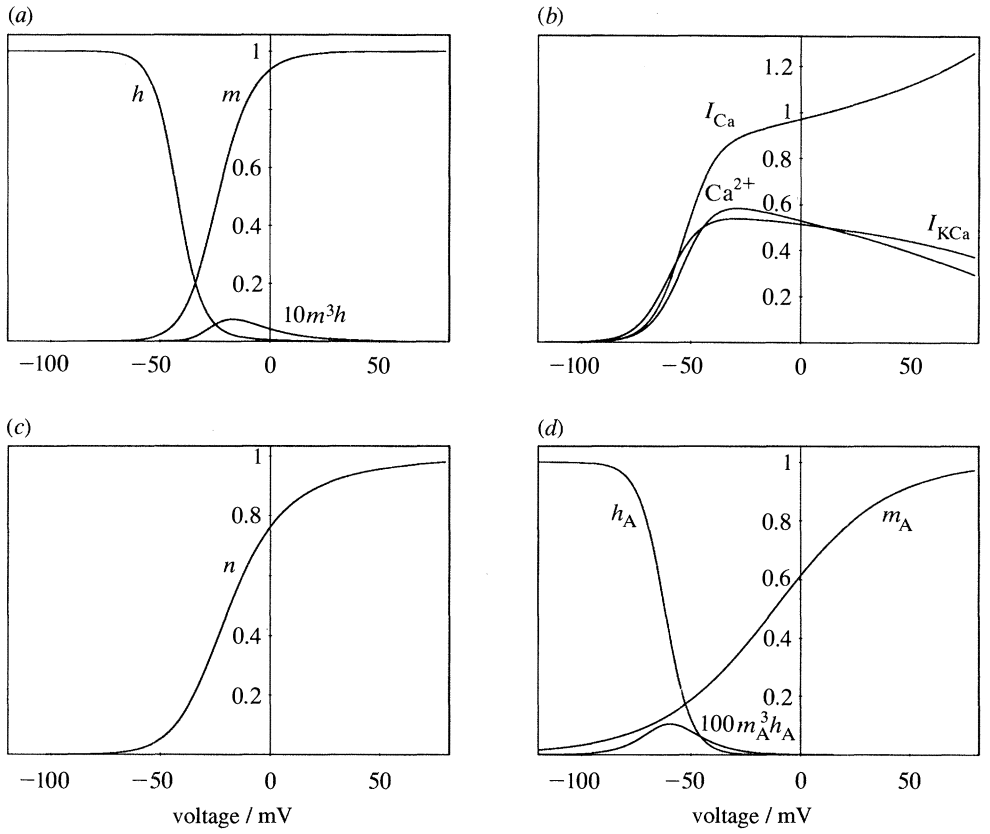

Figure 1. (*a*) The steady state characteristics of the sodium Na channels are plotted. The increasing curve is the steady state value of the activation variable m. The decreasing curve is the steady value of the inactivation variable h. The curve with the maximum near $v = -20$ is the product $10\,m^3h$ that modifies the conductance of the current i_{Na}. (*b*) The steady state characteristics of the calcium current and the potassium activated current are plotted. The curve with a maximum value approximately 0.6 is the steady state value of intracellular free Ca^{2+} obtained from solving the equation $c = 0$ with $k_{Ca} = 0.0078$. The upper curve gives the steady state values of the factor $z/(0.5 + c)$ that multiplies $g_{Ca}(v - v_{Ca})$ in the expression for the current I_{Ca}. The lower curve gives the steady state values of the factor $c/(0.5 + c)$ that multiplies $g_{KCa}(v - v_{KCa})$ to give I_{KCa}. (*c*) The steady state values of activation variable n of the potassium K channel are shown. (*d*) The steady state characteristics of the potassium A channels are plotted. The increasing curve is the steady state value of the activation variable m_A. The decreasing curve is the steady value of the inactivation variable h_A. The curve with the maximum near $v = -60$ mV is the product $100\,m_A^3h_A$ that modifies the conductance of the current i_A.

(equation (6)) used here follows its representation by Hodgkin–Huxley. There is no significant inactivation process for this channel. The activation variable is denoted n (defined by the differential equation (8) together with equations (17) and (18)) and the conductance of the channel is given by the expression $g_K n^4$. The potassium equilibrium potential is denoted v_K. Figure 1*c* shows the voltage dependence of the potassium steady-state-value activation.

4. The second type of potassium current incorporated in our model is a channel whose activation is influenced by the concentration of intracellular free calcium. Gorman and Thomas (1978) demonstrated that changes in the permeability of the cell membrane to K^+ ions due to changes in intracellular free calcium concentration play an important role in bursting of the Aplysia R15 neuron. We have used the representation of the calcium-activated potassium channel (equations (6), (7), (10) and (21)) as described in the paper of Rinzel and Lee (1987). The change in the conductance of the channel due to calcium is given by the factor $c/(0.5 + c)$. The steady state values of this factor are plotted in figure 1*b*. The associated maximal conductance is denoted g_{KCa}. In this formulation, note that the voltage dependence of I_{KCa} arises solely from the voltage dependence of the calcium current I_{Ca}. There are some preparations where I_{KCa} has an additional intrinsic voltage dependence of activation (see Barrett et al. 1982; Hille 1992), but this is not incorporated into our model.

5. A third potassium current is carried by the A channel, which allows a transient outward current to flow following a period of hyperpolarization (Connor & Stevens 1971). Since the incorporation of I_A into our model is a new addition to the Rinzel and Lee model of a bursting neuron (Rinzel & Lee 1987), we describe it in more detail than the other currents. We have taken data on I_A collected by Golowasch (1991) on the A current in the LP cell of the stomatogastric ganglion of the rock crab *Cancer borealis*, and by Tierney and Harris-Warrick (1992) in the AB cell of the stomatogastric ganglion of the spiny lobster *Panulirus interruptus*, as the basis for our representation of this current. The A current can be blocked selectively

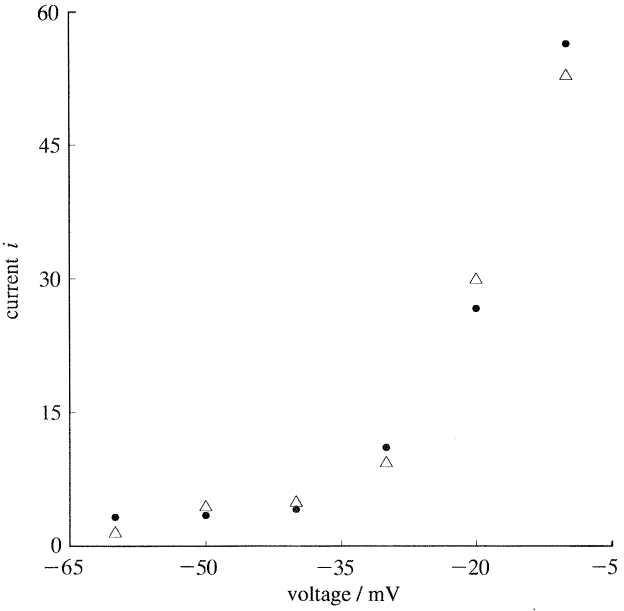

Figure 2. The steady state current voltage relationship of the A current i_A, as measured by Tierney and Harris-Warrick (1992) versus peak measurements from our model. The conductance of the A current has been chosen as 125 μS.

in *Panulirus* stomatogastric neurons by application of 4-aminopyridine (4-AP) (Tierney & Harris-Warrick 1992). Consequently, I_A can be isolated by subtracting the total current measured with and without 4-AP. I_A can also be isolated by a digital subtraction of the evoked leak-subtracted currents from a holding potential where the channels are completely inactivated (typically −50 to −40 mV) from an equivalent set of leak-subtracted currents taken from a holding potential where there is no resting inactivation of I_A (typically −90 to −100 mV) (Golowasch 1991; Tierney & Harris-Warrick 1992). We postulate that the kinetic description of the A channel is similar to that of the sodium channel (i.e. three *a* type and one *b* type gating particles). The voltage dependent variables m_A and h_A characterize activation and inactivation, respectively. The inactivation process is governed by the differential equation (11), with the steady state value h_{Ai} and the rate constant k_A. Because experiments reveal that activation occurs on a much faster time scale than inactivation, it is considered instantaneous in the model. Equations (19) and (20) describe m_A and the steady state value h_{Ai} as sigmoid exponential functions with half maximal values v_a and v_b and widths s_a and s_b respectively. They are derived by a fit to the experimental data of Golowasch (1991) and of Tierney and Harris-Warrick (1992), and differ from the model used by Golowasch (1991) and by Buchholtz *et al.* (1992). Figure 2 shows our calculation of the conductance of the A channel from these data. In contrast to its apparent weak role in the dynamics of the LP cell (Golowasch 1991), the A current plays a crucial role in the bursting patterns of the AB cell (Harris-Warrick & Johnson 1987). This conclusion is based on experiments on the isolated AB cell in which the A channels were increasingly blocked by increasing concentrations of 4-AP (Tierney & Harris-Warrick 1992; figures 7 and 9). Increasing blockade of I_A shifts the isolated AB cell from a silent quiescent state (figures 7*a* and 9*a*) to an oscillating state (figures 7*c*, *d* and 9*b–d*) to tonic firing (figure 7*e*) or silence (figure 9*e*), while it only yields a relatively small depolarization of the LP cell (Golowasch 1991; Buchholtz *et al.* 1992). The pronounced effect of the A current is obtained in our model by assigning a relatively large 'maximal conductance' to the A current term. The constant g_A represents the conductance corresponding to a fully activated channel with no inactivation. Figure 2 shows the peak current-voltage relationship for I_A, as measured experimentally (Tierney & Harris-Warrick 1992) versus the numerical computations from our model. In figure 1*d* we display the voltage dependence of the activation process, the inactivation process, and the expression $100\, m_A^3 h_A$, (normalized A conductance, for a typical value $g_A = 100$ μS).

6. The final current included in our model represents the leak current (I_l) of the membrane. These are background currents, mainly due to chloride, whose conductance is assumed to be voltage independent. The parameters affecting this current are its conductance (g_l) and equilibrium potential (v_l).

Our model is thus defined by the following set of equations where the differential equations (equations (6–11)) appear first, grouped together, followed by equations (12–20) which describe the instantaneous processes and the steady state values. Finally, equation (21) is related to the calcium kinetics.

$$C_m \dot{v} = -\Bigg(\underbrace{g_{Na} m^3 h (v - v_{Na})}_{I_{Na}} + \underbrace{g_{Ca} \frac{z}{0.5 + c}(v - v_{Ca})}_{I_{Ca}} + \underbrace{g_K n^4 (v - v_K)}_{I_K} + \underbrace{g_{KCa} \frac{c}{0.5 + c}(v - v_K)}_{I_{KCa}} + \underbrace{g_A m_A^3 h_A (v - v_K)}_{I_A} + \underbrace{g_l (v - v_l)}_{I_l}\Bigg) + I_{ext} \quad (6)$$

$$\dot{c} = \rho\left(\frac{(k_{Ca} z (v_{Ca} - v)}{(1 + 2c)} - c\right) \quad (7)$$

$$\dot{n} = \lambda_n (a_n (1 - n) - b_n n) \quad (8)$$

$$\dot{h} = \lambda_h (a_h (1 - h) - b_h h) \quad (9)$$

$$\dot{z} = (z_v - z)/\tau_z \quad (10)$$

$$\dot{h}_A = (h_{Ai} - h_A) k_A \quad (11)$$

$$a_m = \frac{\frac{127}{105} v + \frac{201}{7}}{10 - 10 e^{-\frac{201}{70} - \frac{127}{1050} v}} \quad (12)$$

$$b_m = 4 e^{-\frac{188}{63} - \frac{127}{1890} v} \quad (13)$$

$$m = \frac{a_m}{a_m + b_m} \quad (14)$$

$$a_h = \frac{7}{100} e^{-\frac{94}{35} - \frac{127}{2100} v} \quad (15)$$

$$b_h = \frac{1}{1 + e^{-\frac{83}{35} - \frac{127}{1050} v}} \quad (16)$$

PHILOSOPHICAL TRANSACTIONS OF THE ROYAL SOCIETY B BIOLOGICAL SCIENCES

$$a_n = \frac{\frac{127}{105}v + \frac{166}{7}}{100 - 100e^{-\frac{83}{35} - \frac{127}{1050}v}} \tag{17}$$

$$b_n = \frac{1}{8}e^{-\frac{59}{140} - \frac{127}{8400}v} \tag{18}$$

$$m_A = \frac{1}{1 + e^{\frac{v - v_a}{s_a}}} \tag{19}$$

$$h_{Ai} = \frac{1}{1 + e^{\frac{v - v_b}{s_b}}} \tag{20}$$

$$z_v = \frac{1}{1 + e^{-\frac{15}{100}(v - z_b)}} \tag{21}$$

To complete the description of the model table 1 gives the values we used for the parameters that appear in equations (6–21). We quote here only those parameters which were held fixed throughout the analysis. The ranges of the parameters g_A and g_{KCa} are discussed in § 4. The units of all conductances are μS.

3. MODEL ANALYSIS

Realistic models for the responses of neurons constructed from currents conducted by several ion channels yield multidimensional systems of ordinary differential equations containing complicated analytic expressions and many different parameters. The system given above is a typical example. It is difficult to predict the activity of such a model neuron from inspection of the differential equations defining it. Computer simulations of the model predictions are required. There is no other way than numerical integration to amalgamate the information about different currents, although it is possible after the fact to give a qualitative description of the dynamics in terms of their activation and inactivation processes.

Table 1. *Values of parameters that appear in equations (6–21)*

parameter	value	units
ρ	0.003	ms^{-1}
λ_n	0.8	ms^{-1}
λ_h	0.8	ms^{-1}
k_A	1	ms^{-1}
τ_z	23.5	ms
k_{Ca}	0.0078	mV^{-1}
z_b	−50	mV
v_a	−12	mV
v_b	−62	mV
s_a	−26	mV
s_b	6	mV
v_{Na}	30	mV
v_{Ca}	140	mV
v_K	−75	mV
v_l	−40	mV
g_l	0.0854	μS
g_K	8.0	μS
g_{Ca}	0.04	μS
g_{Na}	15	μS
C_m	1	nF

Dynamical systems theory (Guckenheimer & Holmes 1983) can be used to guide these simulations in a systematic manner.

Numerical integration of individual trajectories presents no unusual computational problems, but the characterization of how the dynamical behavior of a model depends upon its many parameters is a formidable task. In this paper, we introduce the analysis of neural models with methods that rely upon bifurcation theory. By studying properties of dynamical systems that depend upon parameters, patterns of bifurcation are identified that show how qualitative changes in the phase portraits of the vector fields occur as parameters are varied. Some types of bifurcations can be identified in neuronal models using tools from computer algebra systems. The calculation of degenerate bifurcations with the computer program Maple (Char *et al.* 1991) allows us to readily locate regions of parameter space in which the models have complex dynamical behavior similar to that seen in biological experiments with the AB neuron. The information about equilibria derived from these calculations is inserted into an interactive environment for visualizing trajectories computed by numerical integration (Back *et al.* 1992). The analysis of the unfoldings of degenerate bifurcations can also be used to locate parameter regions with a rich repertoire of dynamical behavior.

The explicit calculation of bifurcations of equilibrium points has been an important part of our investigations. Therefore, we describe how these mathematical calculations were performed. (For those with little interest in mathematical detail, the remainder of the paper is independent of this description.) If $\dot{x} = f_\lambda(x)$ is a vector field depending upon parameters, then the equations describing bifurcations of an equilibrium of the vector field are given by $f_\lambda(x) = 0$ together with conditions on the Jacobian derivative Df of f. For saddle-node bifurcations, the condition is that Df have a zero eigenvalue, or equivalently that the determinant of Df be zero. For Hopf bifurcations, the condition is that Df have a pair of pure imaginary eigenvalues. The eigenvalues are roots of the characteristic polynomial of Df. Since the characteristic polynomial is real, the sum of a pair of pure imaginary eigenvalues is zero. The condition that the characteristic polynomial have a pair of roots with zero sum can be described by a (complicated) polynomial in the coefficients of the characteristic polynomial of Df (Guckenheimer *et al.* 1993). Whether the pair of roots are real or pure imaginary can be determined by an inequality involving the coefficients of the characteristic polynomial. In general, one does not expect explicit analytic expressions for the solutions to the multidimensional systems of equations yielding equilibrium points. In the case of neuron models, however, the complexity of the analytic expressions is largely in the dependence of f on the membrane potential v and in the nonlinear dependence of $\dot{v}$ on the remaining variables in the system. When an equilibrium is known to occur with potential v_0, it is easy to solve for the equilibrium values of the remaining variables. We exploit this fact

PHILOSOPHICAL TRANSACTIONS OF THE ROYAL SOCIETY B BIOLOGICAL SCIENCES

in our computations. Furthermore, $\dot{v}$ has a simple dependence on many of the system parameters such as maximal conductances for the different channels and the equilibrium potentials of different ions. Thus we can solve for the parameter values that lead to equilibria at specific values of v by treating v as an independent variable. We solve for the equilibrium values of the remaining variables and parameters that lead to solutions of the equation $\dot{v}=0$ and the desired bifurcation equation(s). By carrying through these calculations for different values of v and leaving two parameters undetermined at the start of the calculation, we determine curves in a two dimensional parameter space at which Hopf and saddle-node bifurcations (Guckenheimer & Holmes 1983) occur.

The data obtained from the symbolic computation programs was edited into a format used by the program *DsTool* (Back *et al.* 1992) for labeling parameter values. This program provides an efficient environment for the interactive exploration of dynamical systems. Of particular interest for this study, *DsTool* provides a graphical window in which points from a two dimensional slice of the parameter space of the system can be marked with symbols and the asymptotic dynamical behavior of the corresponding trajectories observed visually. We have used this facility to label the bifurcation points of parameter space that were computed using Maple. The resulting diagram forms a 'template' that divides the parameter space into regions with different dynamical behavior. The numerical integration routines of *DsTool* were then used to compute and display the corresponding trajectories. Visual inspection of the asymptotic behavior of the trajectories led to further divisions of the parameter space into regions with (apparently) different dynamical behavior.

4. RESULTS

Our goal in these computational studies has been to elucidate how the dynamics of the AB neuron model depend upon variations of its parameters. We were particularly interested in identifying and studying regions in the parameter space where small changes in the parameters produce qualitative changes in the behavior of the model, as was seen with a real AB neuron during application of channel-blocking agents and neuromodulators. To achieve this goal, we have constructed maps of the parameter space showing bifurcations between regions with qualitatively different electrical behavior. These maps could then serve as templates for the analysis of changes in the intrinsic activity of conditionally bursting neurons upon exposure to drugs and neuromodulators. Our computational environment allows us to easily manipulate two parameters at once. Following preliminary studies designed to identify the parameters upon which the model is most sensitive, we concentrated on studying simultaneous variations of the parameters g_{KCa}, g_A that represent the maximal conductances of the calcium-activated potassium current and the transient potassium A current. Decreases of these parameters correspond to experiments in which we applied selective potassium channel blockers to an isolated AB cell (Harris-Warrick & Johnson 1987; Tierney & Harris-Warrick 1992).

We start by describing the procedure we used to obtain estimates for the values of the parameters used in the model. Our experimental data were collected by recording currents and voltages intracellularly from the soma of the AB cell. When the voltage clamp procedure is used to study currents in the AB cell, only outward and leak currents are detected (Golowasch 1991; Tierney & Harris-Warrick 1992). This occurs because the AB cell has a very extended neuropil which is not adequately voltage clamped with our procedures. The ion channels for inward currents carried by sodium and calcium ions appear not to be present on the cell body. We assume that they are selectively localized in the neuropil, beyond the region of adequate space clamp. Thus, we cannot obtain direct data for the inward currents in the model. Assuming the values of the equilibrium potentials and the description of the kinetic processes, choices must be made for the maximal conductances g_l, g_K, g_{KCa}, g_A, g_{Ca} and g_{Na}. We have adapted the models of Rinzel and Lee (1987) for the calcium channel and calcium-activated potassium channel. The kinetic parameters of I_{Ca}, c and I_{KCa} have been adjusted to account for the typical 1 s period of the AB cell slow oscillations as contrasted with the 10 s period of the slow oscillations in the Aplysia R15 cell studied by Rinzel and Lee. Ad hoc values were chosen for the leak current. This leaves us with unknown values for the three parameters g_K, g_{KCa}, g_A, representing the maximal conductances of the three potassium channels. Variations of these three parameters correspond to the experimental results of Harris-Warrick and Johnson (1987) who added selective antagonists of these channels to induce rhythmic bursting in an isolated AB neuron. The conductances depend on the conductivity of an individual channel and on the number of channels that are found on the cell's membrane. Since our experimental measurements have limited accuracy due to the space clamp problems discussed above, and since a natural biological variation in the activity of the AB neuron is found in different preparations, we did not try to find exact values for the conductances. Instead, we estimated the range of values they may take while remaining in a plausible region that can represent the the cell's behavior. These estimates were obtained by analysis of experimental data and exploration of the model dynamics.

Figure 3 shows a bifurcation analysis of two dimensional slices of the parameter space in which the axes are one of the pairs (g_{KCa},g_A), (g_K,g_A) or (g_K,g_{KCa}). Points of Hopf and saddle-node bifurcations are drawn on these figures at locations that have been computed by solving systems of seven equations in seven unknowns with the computer algebra system Maple. These equations are obtained by setting the right hand sides of Equations (6–11) to 0 and adding one additional equation for detecting the presence of a bifurcation as described in the previous section. The saddle-node bifurcations are marked by crosses and the Hopf bifurcations are marked by points. The

PHILOSOPHICAL TRANSACTIONS OF THE ROYAL SOCIETY B BIOLOGICAL SCIENCES

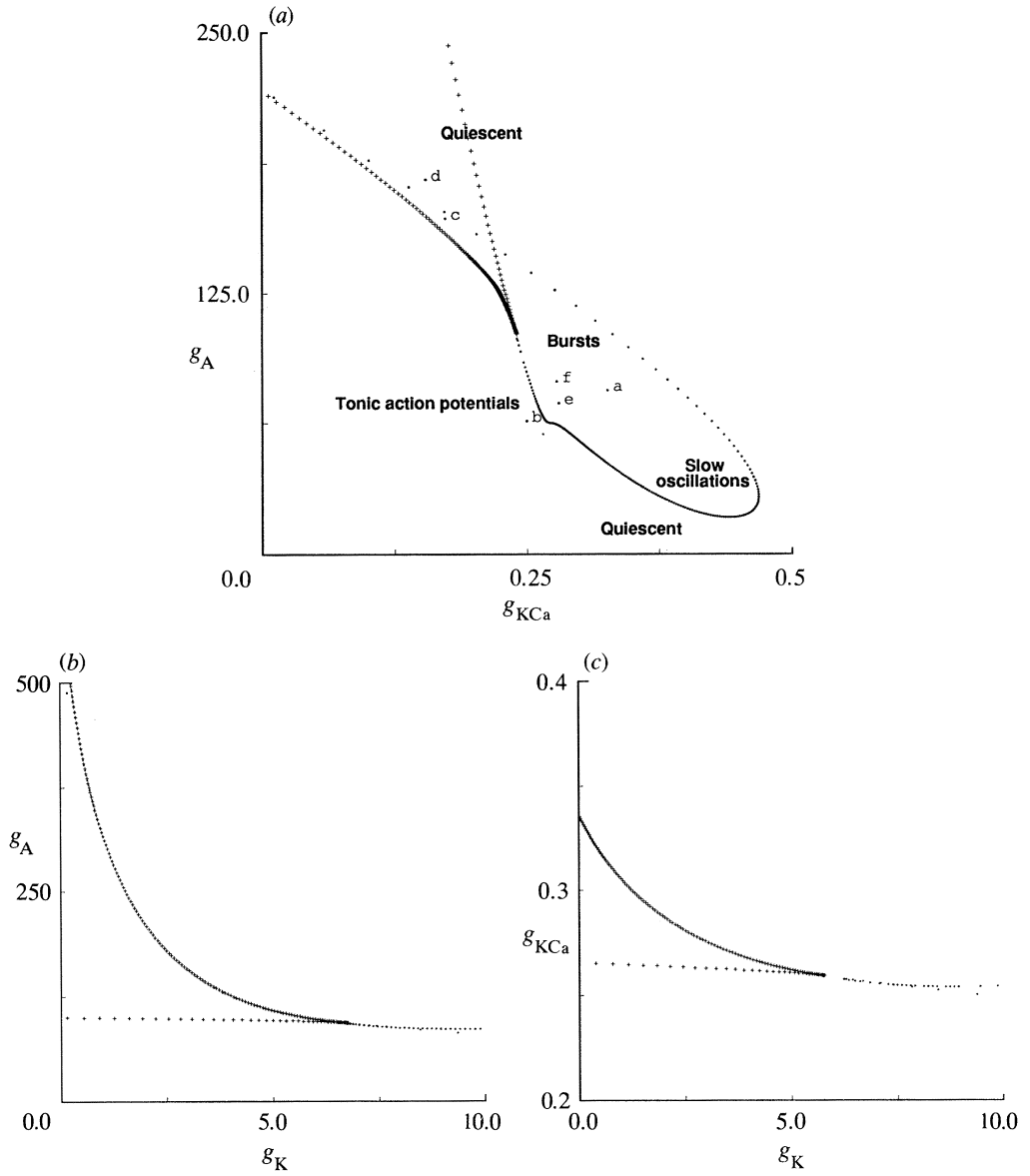

Figure 3. Two dimensional slices in the parameter space showing data on saddle-node and Hopf bifurcations. The crosses denote saddle-node bifurcations and the dots denote Hopf bifurcations. The data shown were computed using the program Maple. (*a*) Bifurcations in the (g_{KCa},g_A) plane. Patterns of activity of the model in different regions of parameter space are noted. (*b*) Bifurcations in the (g_K,g_A) plane with $g_{KCa}=0.25$. (*c*) Bifurcations in the (g_K,g_{KCa}) plane with $g_A=100$. Note that there is much less dependence of the bifurcations on the delayed rectifier conductance g_K than on the conductances (g_{KCa} and g_A).

curves of Hopf and saddle-node bifurcations form boundaries between regions of the parameter space with qualitatively different dynamical behavior.

As the conductances of the potassium channels are varied, the behavior of the model cell is observed to vary. One can form a rough classification into four different types of observed states: quiescent, periodic with a fast period corresponding to tonic action potentials, periodic with a slow period and no action potentials, and bursting behavior which has both slow periodicity and bursts of action potentials during the depolarized phase of the slow oscillations. This classification can be refined: during bursting behavior, the number of action potentials per cycle varies considerably. Additionally, there are complex bursting states with different numbers of action potentials in each cycle that are presumably chaotic. Quantitative aspects of the behavior such as the membrane potential of the quiescent state, the period of the oscillation and the fraction of the period that is part of a bursting cycle are important biological parameters that affect the simple rhythmic behavior driven by the pyloric network.

Using the information from the bifurcation analysis as a template, we investigated the dynamics of trajectories with parameters chosen in different regions of the (g_{KCa},g_A) parameter plane. Some of these trajectories are displayed in figures 4 and 5. The different parameter values used to calculate trajectories figures 4*a–f* and 5*a–f* are displayed by lettered labels on figure 3*a*. Figure 4 shows graphs of voltage versus time (calcium versus time for one case) that can

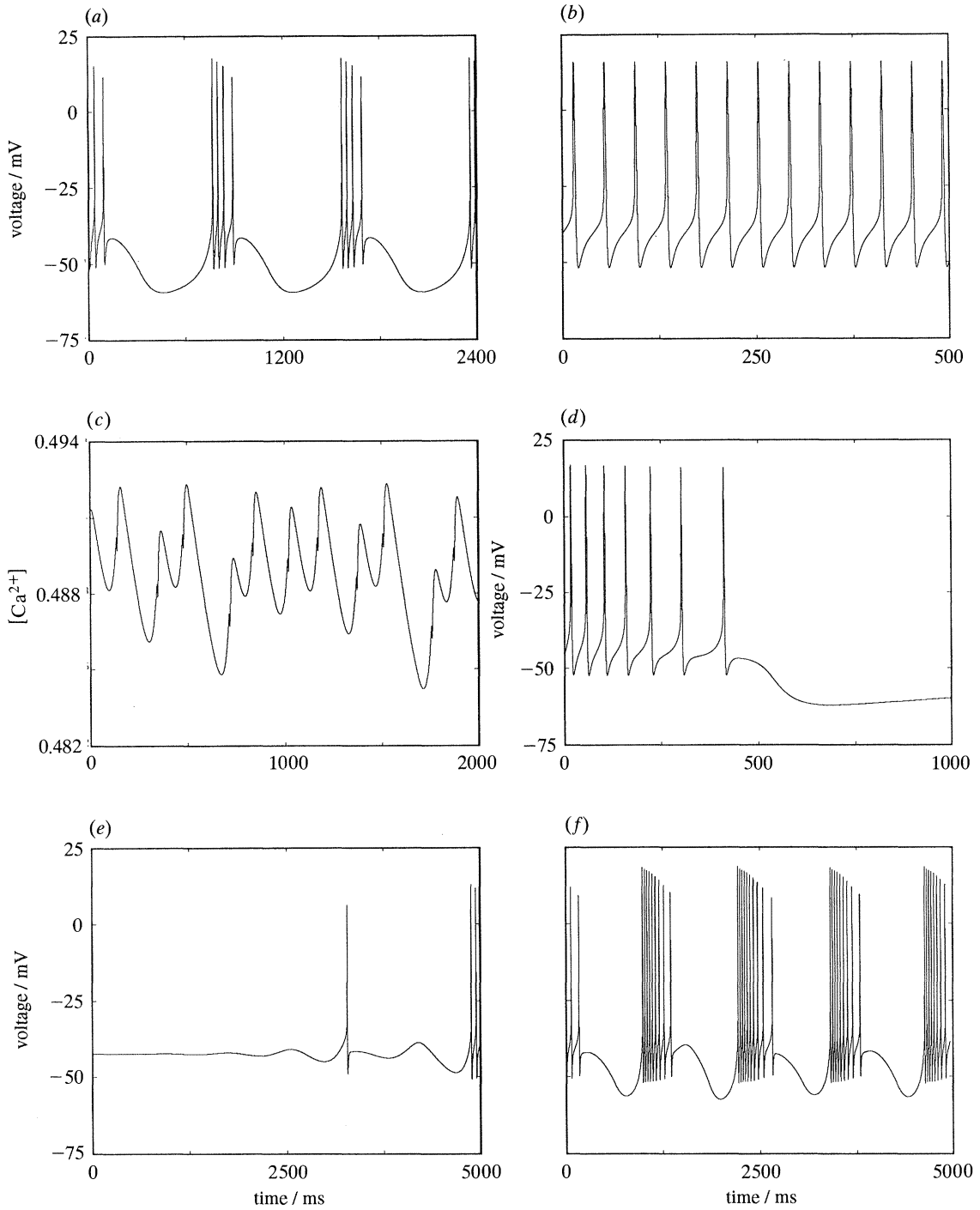

Figure 4. The graphs of voltage versus time for five different parameter values of the model and the graph of calcium concentration versus time for one parameter value. Each trajectory has been run for long enough to give apparent transients time to decay, except for (*d*) where the asymptotic approach to a stable equilibrium state is shown. The values of the parameters other than g_A and g_{KCa} are given in table 1. (*a*) $g_A = 77.95$ and $g_{KCa} = 0.321606$ produces a typical periodic bursting cycle with a period approximately 1 s. (*b*) $g_A = 63.21$ and $g_{KCa} = 0.245336$ produces periodic, tonic action potentials with a period approximately 40 ms. (*c*) $g_A = 164.43$ and $g_{KCa} = 0.16835$ produces a chaotic pattern of action potentials. Calcium concentration versus time is plotted since the voltage appears almost periodic. (*d*) $g_A = 179.7$ and $g_{KCa} = 0.149839$ leads to a quiescent, stable equilibrium. A transient approaching the stable equilibrium is shown. (*e*) $g_A = 71.73$ and $g_{KCa} = 0.2757$ appears close to a homoclinic cycle, a trajectory that starts near an unstable equilibrium and returns close to the equilibrium. The subsequent bursting cycle is chaotic. (*f*) $g_A = 82.07$ and $g_{KCa} = 0.273537$ shows a chaotic trajectory with a variable number of action potentials per bursting cycle.

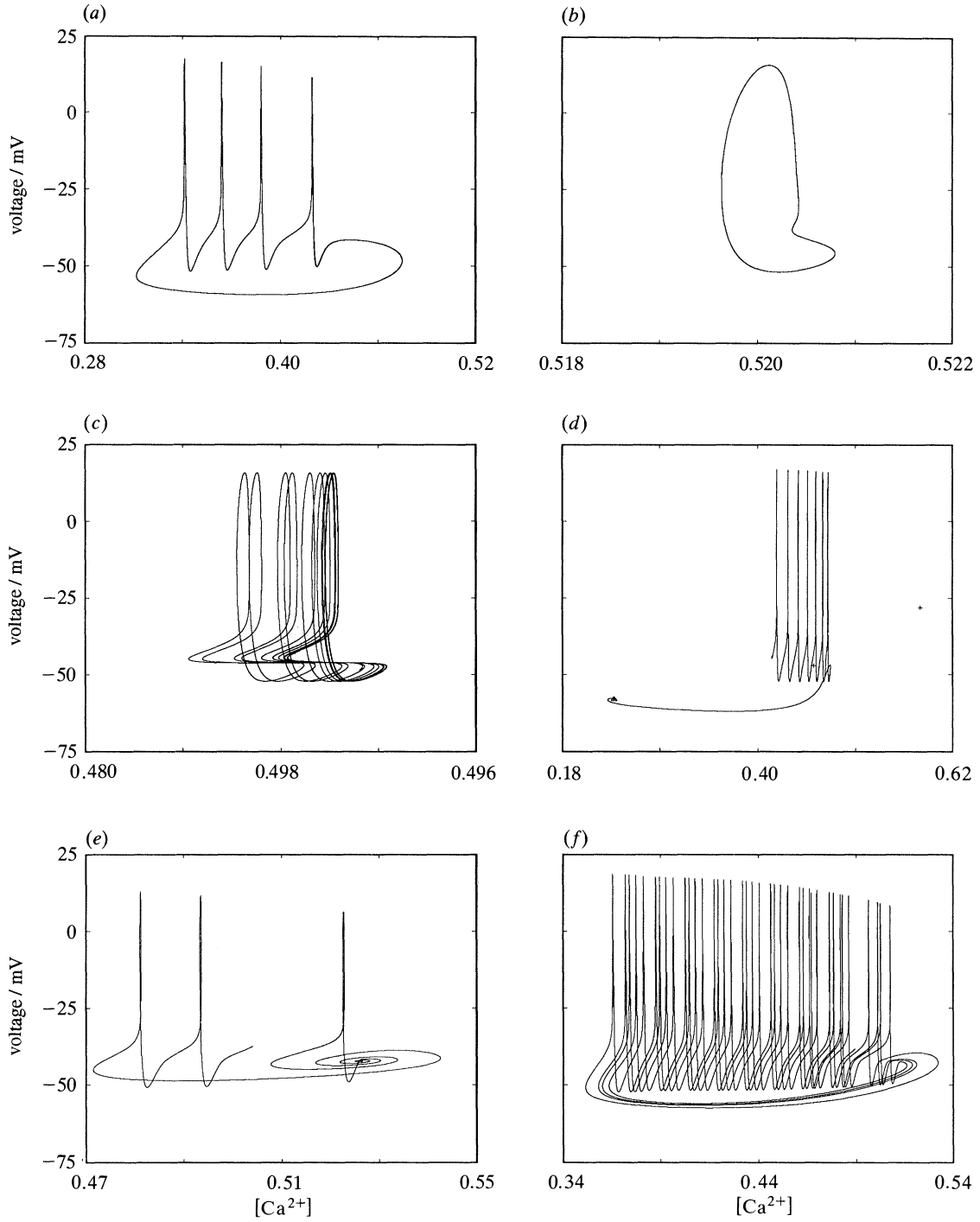

Figure 5. Plots of voltage vs calcium for the same model trajectories shown in figure 3. In (*d*), the triangle denotes the stable equilibrium point, and the crosses locate the projection of two unstable equilibrium points onto the (*Ca*,*v*) plane.

be compared directly to experimental voltage recordings from the AB cell. Since the concentration of intracellular free calcium changes more slowly than the other variables, it is an important determinant of the properties of the slow oscillations. Therefore, we present in figure 5, plots of voltage versus calcium concentration for the same trajectories shown in figure 4.

We describe the major features revealed by this analysis of the (g_{KCa},g_A) parameter plane. There is a region of parameters in which the cell displays bursting behavior or slow oscillations without action potentials. The boundary of this region is approximated by (but not coincident with) the large loop of Hopf bifurcations. Figures 4*a* and 5*a* show a periodic bursting trajectory with four action potentials per burst. The region of tonic action potentials in the parameter plane lies to the left of the 'tail' in the Hopf bifurcation curve that extends down from the loop of bifurcations, intersecting the g_{KCa} axis near $g_{KCa} = 0.3$. Figures 4*b* and 5*b* show a periodic trajectory with tonic action potentials. In some regions, the mechan-

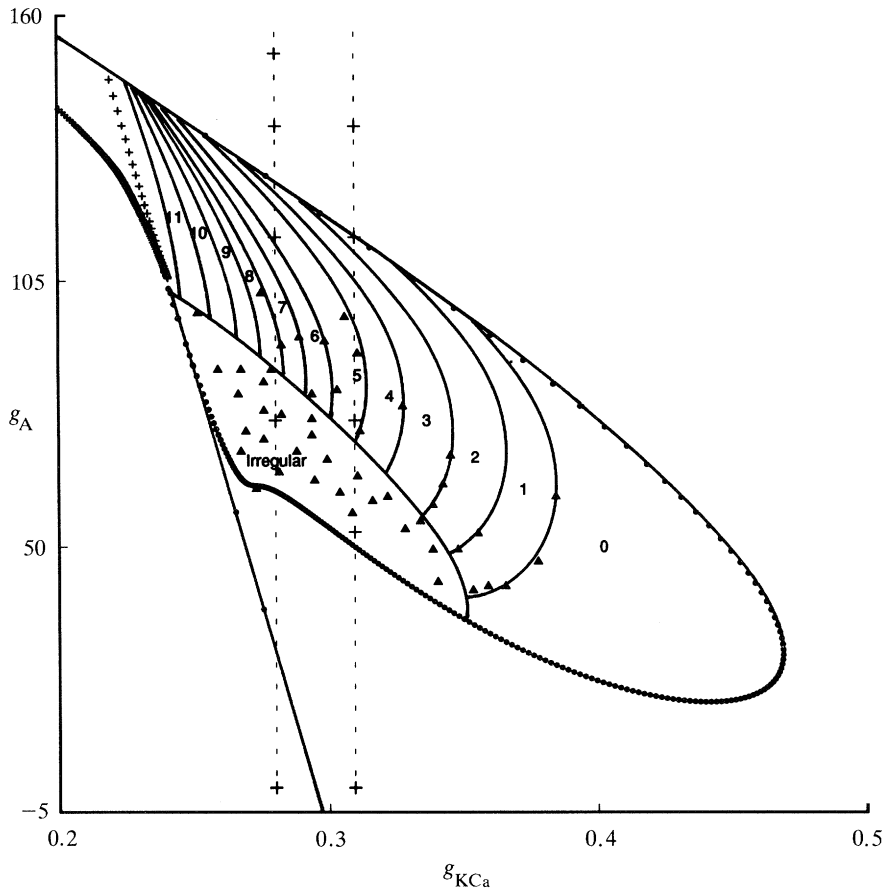

Figure 6. Map of parameter space showing the region of figure 3*a* with underlying slow oscillations divided into subregions with different numbers of action potentials per burst. The numbers label the number of action potentials per burst in each region. The triangles label points at which irregular bursting behavior was observed, either more complex periodicity or chaotic behavior. The large crosses label parameter values used in the comparison between model data and experimental records shown in figures 7 and 9.

isms by which the tonic action potentials disappear are complex. Figures 4*c* and 5*c* show a trajectory near this boundary in which the voltage trace is approximately periodic, but the concentration of intracellular free calcium appears to be chaotic. The region to the right of the tail in the Hopf bifurcation curve and outside the loop of Hopf bifurcations has a stable quiescent state. Figures 4*d* and 5*d* show a trajectory that goes through one burst before settling at a quiescent state. Note that the parameter values associated with figure 5*d* are chosen inside the cusp curve of saddle-nodes in the bifurcation diagram. Here there are three equilibrium states, but only one is stable.

By more extensive sampling of parameter values and initial conditions for numerical integrations of trajectories, we produced a more refined division of the parameter space into regions with different types of attracting states supporting oscillations. Figure 6 shows the division of the region with slow oscillations and bursting behavior into regions with different numbers of action potentials per burst. These regions have been mapped by inspecting trajectories with randomly chosen initial conditions at a large number of different parameter values within the region. There is a general trend for the number of action potentials per burst to increase with decreasing conductance of the calcium activated potassium concentration, although the shape of the regions is hardly regular.

The final step in our study was to make explicit comparisons between a real AB neuron with the behavior of our model during sequential changes in a single parameter. Our computational results give clear predictions about the response of the AB cell to variations in its potassium conductances. These predictions are qualitatively consistent with the experimental findings of Harris-Warrick and Johnson (1987) and Tierney and Harris-Warrick (1992). Their experiments involved addition of selective potassium channel antagonists to a quiescent AB cell. A number of antagonists induced rhythmic bursting, including 4-aminopyridine (a selective blocker of I_A), tetraethylammonium ion (which blocks I_K and I_{KCa}), apamin (which partially blocks I_{KCa}) and a number of conditions which selectively reduce Ca^{2+} entry into the cell (thus blocking I_{KCa}). Although these experiments were qualitative, they suggested that I_A, I_K and I_{KCa} are at least partially active at the normal resting potential, and all that is needed to induce rhythmic bursting is to reduce their currents by reducing the corresponding g_A, g_K or g_{KCa}. In figure 6, for example, the quiescent AB cell can be induced to burst by reductions of g_A, moving the cell vertically down into the

PHILOSOPHICAL TRANSACTIONS OF THE ROYAL SOCIETY B BIOLOGICAL SCIENCES

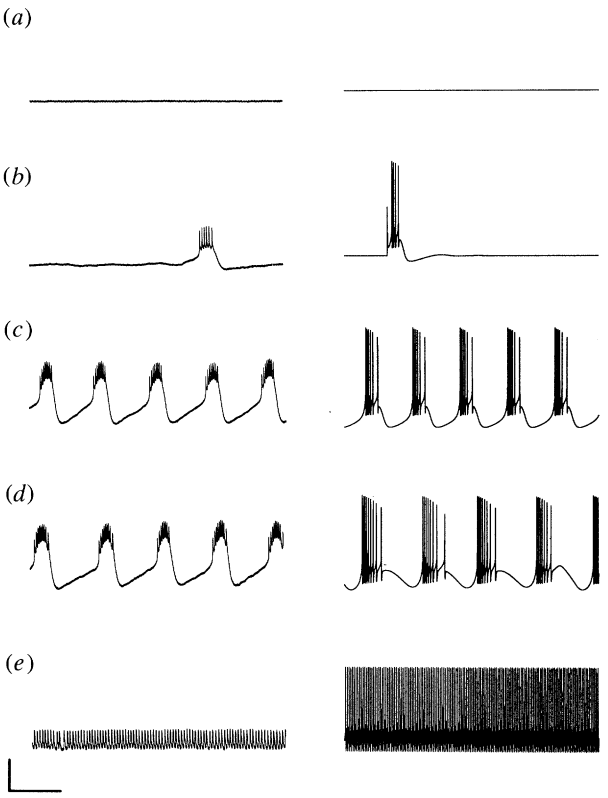

Figure 7. Side by side comparisons between typical experimental time traces of voltage versus time with time traces from the model. The experimental data on the left are taken from a single cell superfused with increasing concentrations of 4-AP. The model data on the right are steady state activity patterns (except for a voltage pulse in (*b*)) taken from a set of parameter values with varying g_A. The value of g_{KCa} is 0.28 and the values of the other parameters are taken from table 1. (*a*) 0 mM 4-AP, $g_A = 152$; (*b*) 0.5 mM 4-AP, $g_A = 136.8$; (*c*) 1.0 mM 4-AP, $g_A = 114$; (*d*) 2.0 mM 4-AP, $g_A = 76$; (*e*) 10.0 mM 4-AP, $g_A = 0$. Left panel markers: 1 s, 15 mV. Right panels show 5 s of traces from the model cell.

region enclosed by Hopf bifurcations. We emphasize that the different channel blockers evoked bursting with very different characteristics (Harris-Warrick & Johnson 1987). This is expected from our model, since each antagonist moves the cell in a different direction of the parameter space, thereby locating the cell in parameter regions with distinct behaviors.

Figures 7 and 8 show a comparison of the responses of an AB neuron and our model to a series of reductions of g_A. The left panels show five traces of voltage versus time recorded from a single isolated AB neuron; these traces were obtained with increasing concentrations of 4-AP (0, 0.5, 1, 2, and 10 mM). The right traces show similar behavior in the model neuron. With reference to figure 6, we choose initial values of $g_{KCa} = 0.28$ and $g_A = 152$ for the quiescent cell model. Starting with these values, we then decreased the value of g_A to 90, 75, 50 and 0 percent of normal, respectively. These percentages correspond to our estimates of the reduction in the maximum conductance of the A current for the corresponding concentrations of 4-AP in the left panels (Tierney & Harris-Warrick 1992). The asymptotic state of the model is shown in the right panels. We have indicated the corresponding values of (g_{KCa}, g_A) as the left hand series of crosses in the map of parameter space for the model neuron shown in figure 6.

In the absence of 4-AP, both the experimental neuron and the model cell are initially in a quiescent state (figure 7*a*). When a tonic depolarizing current, I_{ext}, of 0.5 nA is applied, both the neuron and the model respond by firing a few action potentials before finding a new quiescent equilibrium at a depolarized membrane potential (figure 8*a*). With 0.5 mM 4-AP (90% of initial g_A), the AB neuron shows an unstable quiescent equilibrium that is slightly depolarized from the previous resting potential, and fires an occasional single burst of action potentials (figure 7*b*). The model also shows the slight depolarization but does not fire bursts of action potentials. We consider it likely that this discrepancy arises from 'noise' in the biological system, allowing the AB neuron to occasionally depolarize above threshold to fire a burst. Consistent with this interpretation, a brief depolarizing pulse was given to the model and it responded with a single burst of action potentials as shown in the right hand trace. When I_{ext} (0.5 nA) is applied to either the AB neuron or the model, both respond with the induction of rhythmic oscillation with bursts of action potentials that lasts as long as the current injection (figure 8*b*).

During application of 1 mM (75% g_A) and 2 mM (50% g_A) 4-AP, the AB neuron is in the stable bursting region (figure 7*c*,*d*). As 4-AP is increased, the neuron oscillates at a slightly lower frequency, and fires more action potentials per burst (eight in 1 mM 4-AP (figure 7*c*) versus 9 in 2 mM 4-AP). However, note that the third burst of action potentials in figure 7*d* has eight action potentials rather than nine, so the bursting is not regular. The model cell displays similar behavior for $g_A = 114$ (figure 7*c*) and $g_A = 76$ (figure 7*d*). With $g_A = 114$, the model cell is periodic, firing six action potentials per burst. When g_A is reduced to 72, the parameter fall in the irregular (chaotic) region of figure 6, and the model cell fires bursts of action potentials in which the number of action potentials per burst varies between six and ten.

For 10 mM 4-AP, $g_A = 0$ (Tierney & Harris-Warrick 1992). Under these conditions, this AB neuron fired tonic action potentials at high frequency (figure 7*e*). The model also fires tonically without the slow oscillations seen in figures 7*c* and 7*d*. As seen in figure 6, the elimination of g_A places the parameters of the model below the region of parameter space where bursting occurs, and now shows tonic activity. The model fires action potentials at a higher rate than the AB neuron; this may reflect the more rapid kinetics of the currents underlying the action potential in our model than in the real cell.

Results similar to those shown in figures 7 and 8 were observed with four isolated AB neurons. However, a fifth cell showed somewhat different responses to reduction in g_A (left panels, figure 9). We hypothesize that this difference arose from the natural biological variability in the properties of the AB cell in different preparations (Harris-Warrick & Flamm 1987; Harris-Warrick & Johnson 1987; Tierney & Harris-Warrick 1992). This difference can be

PHILOSOPHICAL TRANSACTIONS OF THE ROYAL SOCIETY B BIOLOGICAL SCIENCES

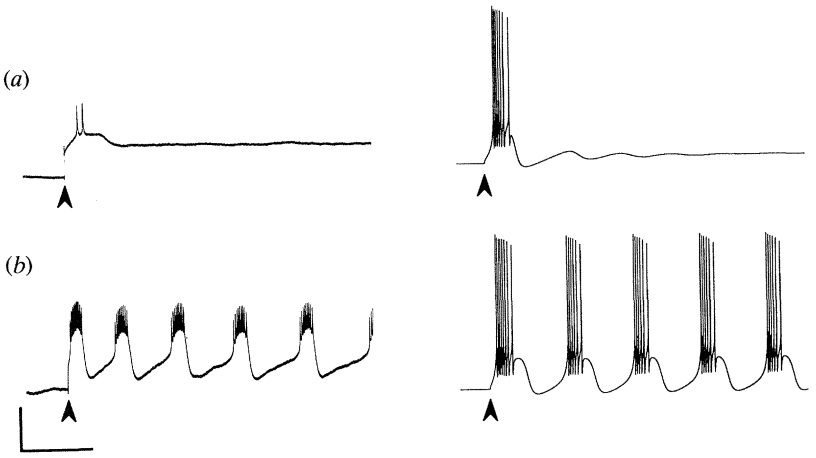

Figure 8. Responses of the AB neuron and model to external current injection. The same neuron and parameter values from figure 7*a* and 7*b*. In each panel, external current injection of 0.5 nA is applied at the arrow and maintained for the rest of the trace. (*a*) 0 4-AP; (*b*) 0.5 mM 4-AP.

modelled by choosing an initial value of g_{KCa} that is slightly different from those in the model cell shown in figures 7 and 8. Based upon figure 6 and the cell's response to 4-AP, we selected a value of 0.309361. The corresponding values of (g_{KCa},g_A) are shown as the right-hand vertical series of crosses in the parameter space for the model shown in figure 6. The five traces in the left panels of figure 9 were obtained from an experiment where the AB cell was bathed with 4-AP concentrations of 0.5, 1, 2, 3 and 10 mM 4-AP (which, respectively, correspond to 90, 75, 50, 35 and 0 percent of the initial value of g_A. The traces showing the asymptotic state of the model at these values of g_A are shown in the right panels of figure 9.

The neuron was quiescent at both 0 (data not shown) and 0.5 mM 4-AP (figure 9*a*); the only difference was a slight depolarization of the neuron with 0.5 mM 4-AP, which is duplicated with the model for 90% of the normal g_A for this cell. At 1 mM 4-AP, the AB neuron oscillated irregularly, and with a low number of action potentials per burst (4–5 in figure 9*b*). When the g_A value was reduced to 75% of its initial value of 152, the model cell was periodic, firing two action potentials per burst.

At 2 mM 4-AP (corresponding to 50% of initial g_A), this AB neuron fired rhythmically at a higher frequency, with seven action potentials per burst (figure 9*c*). The model produces a similar result: the cell is still periodic, with a higher frequency and a larger number of action potentials per burst (five). As g_A was further reduced by increasing the concentration of 4-AP to 3 mM, the AB neuron entered a region of unstable bursting, with bursts containing variable (but smaller) numbers of action potentials (figure 9*d*). The model shows very similar behavior with $g_A = 53$, corresponding to 35% of the initial g_A value. The model cell is irregular, oscillating in a manner that reaches threshold for firing action potentials on some cycles, but not others. When the cell fires action potentials, it fires one or two per burst. This reduction in the number of action potentials per burst is consistent with the smaller number of action potentials per burst of the biological AB neuron in 3 mM 4-AP (figure 9*d*) compared with 2 mM 4-AP (figure 9*c*). Finally, elimination of g_A with 10 mM 4-AP caused this neuron to fall silent (figure 9*e*). The model predicts the identical result.

The general properties of the model in this parameter range match these experimental data well. Based on an analysis of the parameter space in figure 6, our model predicts that the second neuron (figure 9) has a slightly larger value of g_{KCa} than the first neuron (figure 7). Reduction of g_A with application of 4-AP is equivalent to vertical downward movement in the parameter space of figure 6 (see crosses for the values used to represent the model cells). Modest reductions of g_A from the chosen initial value 152 moves both cells into the region of rhythmic oscillations, but with different numbers of action potentials per burst (more in the first neuron (figure 7) than in the second (figure 9). Further reduction of g_A carries the first neuron into the region of tonic activity bounded by a curve of Hopf bifurcations on the right, while the second neuron moves to the region corresponding to quiescent equilibrium activity on the opposite side of this Hopf bifurcation curve (figure 6). Thus, our model predicts appropriate responses of both neurons to increasing concentrations of 4-AP, assuming that their initial parameters of g_{KCa} were slightly different. This is entirely consistent with the subtle variations of electrical activity of the AB neuron in different preparations (Harris-Warrick & Flamm 1987; Harris-Warrick & Johnson 1987; Tierney & Harris-Warrick 1992). We emphasize the ability of our model to mimic this natural variability by selecting appropriate values for the parameters; this is greatly expedited by comparison of the experimental data with thoroughly analyzed maps of parameter space such as the one displayed in figure 6.

Despite the agreement between our model and these experimental data, there remain important differences. Perhaps the greatest discrepancy between the two is the difference in the shape of the voltage versus time recordings in figures 7 and 9. The amplitude of the action potentials within the model is much larger than the amplitude of the action poten-

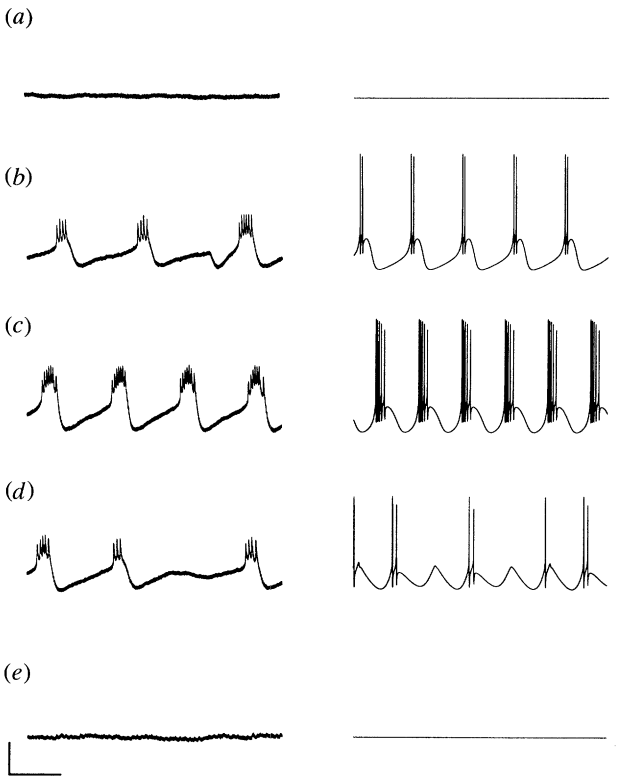

Figure 9. Side by side comparisons between experimental time traces of voltage versus time from a different neuron with time traces from the model. The experimental data on the left are taken from a single cell superfused with increasing concentrations of 4-AP. The model data on the right are taken from a set of parameter values with varying g_A. The value of g_{KCa} is 0.309361 and the values of the other parameters are taken from table 1. (*a*) 0.5 mM 4-AP, $g_A = 136.8$; (*b*) 1.0 mM 4-AP, $g_A = 114$; (*c*) 2.0 mM 4-AP, $g_A = 76$; (*d*) 3.0 mM 4-AP, $g_A = 53$; (*e*) 4.0 mM 4-AP, $g_A = 0$.

tials recorded in the soma of the AB cell. As described above, the soma of the AB cell is electrically inexcitable and lacks the ion channels generating the inward currents of action potentials. Thus the action potentials, generated in the neuropil, propagate passively along a long thin process to the soma. This process acts as a low pass filter, greatly diminishing the spike amplitude of the action potentials while not markedly affecting the amplitude of the slow oscillations. The low amplitude of the experimental spikes is an artifact of the recording site. The second important difference is that there are systematically more action potentials per burst in the AB neurons than in the model cells (for the chosen parameters). Finally, there are differences in the properties of the underlying slow oscillations. The real neuron had a more linear rise of voltage during the recovery phase of the bursting cycle than does the model neuron for the parameter values illustrated here. It also did not exhibit the 'overshoot' after the last action potential of the burst that the model cell predicted. We expect that these differences may be alleviated by further changes in other parameters than the ones that have been the focus of this investigation.

We make a number of more technical comments about the structure of bifurcations and the presence of chaotic behavior in the system, for the benefit of mathematically inclined readers. As one crosses the Hopf bifurcation curve vertically upward in the bursting region near the point (0.309361,114) marked with a large cross in figure 6, unstable periodic orbits emerge at the Hopf bifurcation. There is a region of bistability above the Hopf bifurcation curve (i.e. larger g_A) for which different initial conditions tend to either a stable equilibrium or to a bursting oscillation. These bursting oscillation solutions appear to merge with the family of periodic orbits that bifurcated from the equilibrium at the Hopf bifurcation. In the course of this process, either the stable bursting oscillations become slow oscillations without bursts, or the unstable oscillations develop bursts.

As one moves from the bursting region across the saddle-node curve into the region with multiple equilibria by decreasing g_{KCa} (to the left of the region labeled as having 11 action potentials per burst in figure 6), there is a complex transition from bursting solutions (figures 4*a* and 5*a*) to periodic action potentials (figures 4*b* and 5*b*). Approaching this transition from the left (increasing g_{KCa}), the periodic action potentials appear to go through a transition to aperiodic, but rapid action potentials, that follows the classical 'period-doubling' route to chaos. There is a small region of the parameter space in which the range of variation of the calcium concentration changes chaotically in sequences of action potentials (figures 4*c* and 5*c*). At the boundary of this region, the small variations of the chaotically varying calcium concentration reach a threshold at which the calcium concentration falls to a low value and the membrane potential becomes hyperpolarized for a time that is long compared to the time scale of the action potentials. The calcium concentration eventually begins to increase and the membrane depolarizes, leading to a burst of action potentials during which the calcium concentration further increases. Chaotic action potentials are interspersed with intermittent bursts in this régime.

The Hopf bifurcation curve passes through a point of double Hopf bifurcation along its lower branch. One can interpret the two modes as representing the slow oscillations and the action potentials and view the small loop in the curve of Hopf bifurcations as the parameter regime in which the time scales for these oscillations become comparable. At the point of double Hopf bifurcation, the ratio between the periods of the two oscillations is approximately six (as determined from the eigenvalues computed by the program *DsTool* at the point of double Hopf bifurcation), which is not as large as the typical ratio between the time scales of action potentials and slow oscillations. The period of a typical action potential is approximately 30 ms while the slow oscillations have a period of approximately 1 s. Near a point of double Hopf bifurcation, one expects the possibility of nonlinear interactions of two modes that can be described by a reduction to 'normal form' for the system (Guckenheimer & Holmes 1983). The effect of these nonlinear interactions depends upon coefficients in the normal form equation that we did not try to compute.

PHILOSOPHICAL TRANSACTIONS OF THE ROYAL SOCIETY B BIOLOGICAL SCIENCES

Additionally, the angle between the two curves of Hopf bifurcation is small in the model, making it difficult to see these interactions easily.

The final property of the bifurcation diagram of figure 6 that we comment upon is the presence of a curve of 'homoclinic bifurcation' associated with chaotic trajectories in the region that is labeled 'irregular'. Silnikov and later Tresser (Guckenheimer & Holmes 1983) analyzed the properties of dynamical systems in which there was a trajectory asymptotic to an equilibrium point in both forwards time and backwards time. Generically, the approach to the equilibrium occurs in the directions for which the linearization has the slowest rate of approach (in both forward and backwards time). There are several different cases distinguished by whether the trajectories approach the equilibrium in an oscillatory fashion or from a well defined direction, and by the ratio of the rates of approach. In the system studied here, the homoclinic orbit that we identify leaves an equilibrium in an oscillatory manner with a slower rate than it approaches it. One expects to find chaotic trajectories in the vicinity of the homoclinic orbit. We do indeed find a rather large chaotic area within the bursting region of the parameter space near this homoclinic bifurcation.

DISCUSSION

The main conclusion of our study is that bifurcation analysis can be used to map the behavior of realistic, channel-based models for the response of a conditionally bursting neuron to changes in its environment. We compared the activity of the AB cell in the stomatogastric ganglion of the spiny lobster *Panulirus interruptus* to that of a six dimensional vector field representing six currents in the membrane of this cell. Through computer analysis and simulation, we have produced maps that illustrate the response of the model to variations in the conductances of the potassium channels of this cell. These maps give us new insight in our studies of how the cell responds to changes in its environment. We are particularly interested in the response of the AB neuron to neuromodulators such as the monoamines dopamine, serotonin and octopamine (Harris-Warrick & R. E. Flamm 1987). In other stomatogastric neurons, these amines appear to modulate the conductances of several potassium currents (Kiehn and R. M. Harris-Warrick 1992; Harris-Warrick *et al.* 1992). Comparison of AB responses to amines and potassium channel antagonists will be greatly facilitated by quantitative reference to maps of the AB cell parameter space (figures 3 and 6).

The repertoire of dynamical behavior displayed by the model neurons is rich and includes chaotic phenomena. Since many of the details of the bifurcations observed in the models require careful analysis of numerically integrated trajectories, matching experimental data with model behavior is still a difficult task. There are many parameters in the model we have explored, and direct measurement of some of these in the AB cell is not yet experimentally feasible. Therefore, determination of parameters that fit well with indirect observations of overall neural activity is an exhaustive task, much of which has not yet been automated. It is more feasible to match a series of neuronal responses to sequential modification of a single variable, as we have done using 4-AP to reduce g_A. This imposes significant constraints on the choice of parameters, hopefully to make them similar to the values in the real cell. For example, in a parameter range $0.15 < g_{KCa} < 0.6$, there are no fewer than ten different sequences of changes in the qualitative rhythmic patterns produced by the model during reductions of g_A. The ranges of parameter values for the conductance g_{KCa} that do match the data are relatively narrow. The two dimensional parameter space map illustrated in figure 6 provides an essential tool for making a successful match between the model and the experimental data. Our confidence that this match is meaningful is strengthened by the fact that the model captures important features in the variability of the data between neurons with only small changes in the model conductance of g_{KCa}. Previous studies of neural models have demonstrated the important roles of the A current and the calcium activated potassium current in shaping oscillatory properties of a cell (Connor & Stevens 1971; Gorman & Thomas 1978), but we show how the delicate balance in the relative magnitude of these two conductances influences the complex patterns of rhythmic behavior displayed by a model neuron.

We do not argue that this model has enough structure to represent all observed behavior of the AB neuron. There are noticeable differences in the model and the data in the magnitude of the action potentials. As described above, this is due to the attenuation of the action potentials between their initiation in the neuropil of the AB neuron and the site of recording in the soma. We do not know the extent to which the single compartment model that we are using can be a good representation for the qualitative properties of this neuron, which clearly has important spatial segregation of currents. Moreover, the model does not contain an exhaustive list of all possible ion channels in the AB cell. For example, we have preliminary evidence for a slow hyperpolarization-activated inward current, I_h, in several STG neurons (Golowasch 1991; Kiehn & Harris-Warrick 1992; Harris-Warrick *et al.* 1992). Other oscillatory neurons appear to contain ion channels with very slow activation and inactivation kinetics. These currents are not present in our model, and they may become important to model certain aspects of the oscillatory behavior of the AB cell. Changes in the form of the model may thus be needed to capture all of the AB neuron's responses to changes in its environment, but this can only be determined through exhaustive study of the properties of the model and further comparison with experimental data. What has been demonstrated is that the currents contained in this model are sufficient to explain the complicated sequential modulation of rhythmic patterns that are produced by increasing blockade of the potassium A current by 4-AP. Systematic mapping of the parameter space associated with

PHILOSOPHICAL TRANSACTIONS OF THE ROYAL SOCIETY B BIOLOGICAL SCIENCES

the conductances of the potassium channels that are incorporated in the model has enabled us to understand the range of rhythmic behavior displayed by the model in a substantial region of its parameter space.

There is a final philosophical point that deserves discussion concerning the parameter values that we have chosen for our model. When initiating our studies, we deliberately sought parameter values at which degenerate bifurcations occur. While it appears fortuitous that these parameter values have yielded a good match with experimental observations, there may be evolutionary advantages for a nerve cell to operate in such a region of the parameter space. One of the functions of the nervous system is to be maximally sensitive to its environment and to radically modify its behavior in response to small changes within that environment. Bifurcations locate points of the parameter space at which a small change in parameter values results in qualitative changes in the system behavior. Near degenerate bifurcations, this sensitivity to small parameter changes is even greater, and there are often more regions of different types of qualitative behavior that are accessible nearby. Using a term introduced by Thom (1975), the nerve cell can function as a maximally sensitive signal detector if it operates at a point of the parameter space that is an 'organizing center'. The computation of such points in models is an effective procedure for locating regions in which the models are sensitive to small changes in the model parameters. We speculate that many neurons and/or neural networks have evolved to operate in such regions.

The research of John Guckenheimer was partially supported by the National Science Foundation, that of Shay Gueron by a Rothschild Fellowship, and that of Ronald Harris-Warrick by the National Institutes of Health grant NS17323 and a research grant from the Human Frontiers Science Program Organization. We thank Dr Bruce Johnson for important discussion of the data and Dr Ann Jane Tierney for assistance with the experiments. J.G. and R.H.-W. would also like to thank Dr Avis Cohen for introducing them, and for her foresight in suggesting that this area of research might form the basis for a fruitful collaboration.

REFERENCES

Back, A., Guckenheimer, J., Myers, M., Wicklin, F. & Worfolk, P. 1992 DsTool: computer assisted exploration of dynamical systems. *Not. Am. math. Soc.* **39**, 303–309.

Baesens, C., Guckenheimer, J., Kim, S. & MacKay R. 1991 Three coupled oscillators: mode-locking, global bifurcations and toroidal chaos. *Physica D* **49**, 387–485.

Barrett, J.N., Magleby, K.L. & Pallotta, B.S. 1982 Properties of single calcium-activated potassium channels in cultured rat muscle. *J. Physiol., Lond.* **331**, 211–230.

Buchholtz, F., Golowasch, J., Epstein, I. & Marder, E. 1992 Mathematical model of an identified stomatogastric ganglion neuron. *J. Neurophysiol.* **67**, 332–339.

Char, B.W., Geddes, K.O., Gonnet, G., Leong, B., Monagan, M. & Watt, S. 1991 *Maple V reference manual.* Springer-Verlag.

Chow, S.N., Deng, B. & Fiedler, B. 1988 *Homoclinic bifurcation at resonant eigenvalues.* Knorad-Zuse-Zentrum für Informationstechnik. Preprint SC-88-10.

Connor, J.A. & Stevens, C.F. 1971 Inward and delay outward membrane currents in isolated neural somata under voltage clamp. *J. Physiol., Lond.* **213**, 1–19, 21–30, 31–53.

Epstein, I.R. & Marder, E. 1990 Multiple modes of a conditional neural oscillator. *Biol. Cybern.* **63**, 25–34.

Golowasch, J.P. 1991 Characterization of a stomatogastric ganglion neuron. A biophysical and mathematical interpretation. Ph.D. thesis, Brandeis University.

Gorman, A.L.F. & Thomas, M.V. 1978 Changes in the intracellular concentration of free calcium ions in a pacemaker neurone, measured with the metallochromatic indicator dye arsenazo III. *J. Physiol., Lond.* **275**, 357–376.

Grasman, J. 1987 *Asymptotic methods for relaxation oscillations and applications.* Springer-Verlag.

Guckenheimer, J. & Holmes, P. 1983 *Nonlinear oscillations, dynamical systems, and bifurcation of vector fields.* Springer Verlag.

Guckenheimer, J., Myers, M. & Sturmfels, B. 1993 Computing Hopf bifurcations. (Submitted.).

Guillemin, V. & Pollack, A. 1974 *Differential topology.* Prentice-Hall.

Harris-Warrick, R.M. & Flamm, R.E. 1987 Multiple mechanisms of bursting in a conditional bursting neuron. *J. Neurosci.* **7**, 2113–2128.

Harris-Warrick, R.M. & Johnson, B. 1987 Potassium channel blockade induces rhythmic activity in a conditional burster neuron. *Brain Res.* **416**, 381–386.

Harris-Warrick, R.M. & Marder, E. 1991 Modulation of neural networks for behavior. *A. Rev. Neurosci.* **14**, 39–57.

Harris-Warrick, R.M., Tierney, A.J. & Coniglo, L. 1992 Mechanisms for dopamine-induced phase shifts in the pyloric motor pattern in the lobster stomatogastric ganglion. *Soc. Neurosci. Abst.* **18**, 1055.

Hille, B. 1992 *Ionic channels of excitable membranes.* Sinauer.

Hodgkin, A.L. & Huxley, A.F. 1952 A quantitative description of membrane current and its applications to conduction and excitation in nerve. *J. Physiol., Lond.* **117**, 500–544

Kiehn, O. & Harris-Warrick, R.M. 1992 5-HT modulation of hyperpolarization-activated inward current and calcium-dependent outward current in a crustacean motoneuron. *J. Neurophysiol.* **68**, 496–508.

Kokubu, H. 1988 Homoclinic and heteroclinic bifurcations of vector fields. *Jap. J. appl. Math.* **5**, 455–501.

Marsden, J. & McCracken, M. 1973 *The Hopf bifurcation theorem and its applications.* Springer-Verlag.

Plant, R.E. 1981 Bifurcation and resonance in a model for bursting neurons. J. math. Biol. **11**, 15–32.

Rinzel, J. & Lee, Y.S. 1987 Dissection of a model for neuronal parabolic bursting. *J. math. Biol.* **25**, 653–675.

Rudy, B. 1988 Diversity and ubiquity of K channels. *Neuroscience* **25**, 729–749.

Selverston, A.I. & Moulins, M. 1986 *The Crustacean stomatogastric ganglion.* Springer-Verlag.

Thom, R. 1975 *Structural Stability and Morphogenesis.* W. A. Benjamin.

Tierney, A.J. & Harris-Warrick, R.M. 1992 Physiological role of the transient potassium current in the pyloric circuit of the lobster stomatogastric ganglion. *J. Neurophysiol.* **67**, 1–11.

Received 19 June 1992; revised 11 January 1993; accepted 15 February 1993

PHILOSOPHICAL TRANSACTIONS OF THE ROYAL SOCIETY B BIOLOGICAL SCIENCES